Neurobiology of Disease

Is Optogenetic Activation of Vglut1-Positive Aβ Low-Threshold Mechanoreceptors Sufficient to Induce Tactile Allodynia in Mice after Nerve Injury?

Alexander Chamessian,[1,2,3] Megumi Matsuda,[1] Michael Young,[2] Michelle Wang,[1] Zhi-Jun Zhang,[1] Di Liu,[1] Brielle Tobin,[1] Zhen-Zhong Xu,[1] Thomas Van de Ven,[1] and Ru-Rong Ji[1,2]

[1]Department of Anesthesiology, [2]Department of Neurobiology, and [3]Medical Scientist Training Program, Duke University School of Medicine, Durham, North Carolina 27710

Mechanical allodynia is a cardinal feature of pathological pain. Recent work has demonstrated the necessity of Aβ-low-threshold mechanoreceptors (Aβ-LTMRs) for mechanical allodynia-like behaviors in mice, but it remains unclear whether these neurons are sufficient to produce pain under pathological conditions. We generated a transgenic mouse in which channelrhodopsin-2 (ChR2) is conditionally expressed in vesicular glutamate transporter 1 (Vglut1) sensory neurons (Vglut1-ChR2), which is a heterogeneous population of large-sized sensory neurons with features consistent with Aβ-LTMRs. In naive male Vglut1-ChR2 mice, transdermal hindpaw photostimulation evoked withdrawal behaviors in an intensity- and frequency-dependent manner, which were abolished by local anesthetic and selective A-fiber blockade. Surprisingly, male Vglut1-ChR2 mice did not show significant differences in light-evoked behaviors or real-time aversion after nerve injury despite marked hypersensitivity to punctate mechanical stimuli. We conclude that optogenetic activation of cutaneous Vglut1-ChR2 neurons alone is not sufficient to produce pain-like behaviors in neuropathic mice.

Key words: allodynia; neuropathic; optogenetics; pain

Significance Statement

Mechanical allodynia, in which innocuous touch is perceived as pain, is a common feature of pathological pain. To test the contribution of low-threshold mechanoreceptors (LTMRs) to nerve-injury-induced mechanical allodynia, we generated and characterized a new transgenic mouse (Vglut1-ChR2) to optogenetically activate cutaneous vesicular glutamate transporter 1 (Vglut1)-positive LTMRs. Using this mouse, we found that light-evoked behaviors were unchanged by nerve injury, which suggests that activation of Vglut1-positive LTMRs alone is not sufficient to produce pain. The Vglut1-ChR2 mouse will be broadly useful for the study of touch, pain, and itch.

Introduction

Low-threshold mechanoreceptors (LTMRs) are a heterogeneous class of primary sensory neurons (PSNs) that subserve the sensation of innocuous touch (Zimmerman et al., 2014). Fast-conducting, myelinated LTMRs are known as Aβ-LTMRs, and these comprise the major tactile receptors in the skin (Abraira and Ginty, 2013). In addition to touch, previous studies in humans and rodents have suggested that under pathological conditions such as inflammation or neuropathy, Aβ-LTMRs can also mediate the sensation of pain induced by touch, a phenomenon referred to as mechanical allodynia (Torebjörk et al., 1992; Lolignier et al., 2015). For chronic pain sufferers, mechanical allodynia can be highly disabling because the myriad tactile stimuli of daily living (e.g., clothing brushing against skin) evoke pain.

Despite much study, it is still unknown which type of PSN mediates mechanical allodynia. Mechanical allodynia could result from the sensitization of nociceptors such that innocuous tactile stimuli are able to activate them. Another possibility is that LTMRs, which are normally activated by innocuous tactile stimuli, could gain the ability to signal to central nociceptive circuits after an insult, giving rise to pain from touch (i.e., allodynia)

Received Aug. 12, 2018; revised May 8, 2019; accepted May 22, 2019.

Author contributions: A.C., M.Y., Z.-J.Z., D.L., Z.-Z.X., T.V.d.V., and R.-R.J. designed research; A.C., M.M., M.Y., M.W., Z.-J.Z., D.L., and Z.-Z.X. performed research; A.C., M.M., M.Y., M.W., Z.-J.Z., D.L., B.T., and Z.-Z.X. analyzed data; A.C. wrote the first draft of the paper; A.C., M.M., M.Y., T.V.d.V., and R.-R.J. edited the paper; A.C., T.V.d.V., and R.-R.J. wrote the paper.

This work was supported in part by the National Institutes of Health (Grants R01DE17794 and R01NS87988 to R.-R.J.), Congressionally Directed Medical Research Programs, and the Department of Defense (Grants W81XWH-12-2-0129 and W81XWH-15-2-0046(TV). We thank Yawar Qadri for critical reading of the manuscript.

The authors declare no competing financial interests.

Correspondence should be addressed to Alexander Chamessian at alexander.chamessian@duke.edu.

https://doi.org/10.1523/JNEUROSCI.2064-18.2019

(Latremoliere and Woolf, 2009). To distinguish between these possibilities, it is necessary to activate a single population of PSNs in the context of mechanical allodynia because a natural mechanical stimulus cannot exclusively engage a single type of sensory neuron.

To that end, we developed and characterized a novel transgenic mouse line, Vglut1-ChR2, in which channelrhodopsin-2 (ChR2) is conditionally expressed in vesicular glutamate transporter 1 (Vglut1) sensory neurons, to enable transdermal optogenetic activation of Aβ-LTMRs. We demonstrate that in the Vglut1-ChR2 mouse, ChR2 is expressed in the majority of Aβ-LTMRs as well as some proprioceptors but not in C- or A-nociceptors. We show that optogenetic stimulation of cutaneous Vglut1-ChR2 Aβ-LTMRs elicits non-nociceptive paw withdrawal behaviors in naive mice and is not aversive. Surprisingly, in the setting of nerve-injury-induced neuropathy, optogenetic activation of Vglut1-ChR2 neurons did not produce pain-like behaviors such as licking, jumping, or vocalization and also did not produce aversion, suggesting that *Vglut1*-expressing Aβ-LTMRs alone may not be sufficient to produce pain, even under pathological conditions.

Materials and Methods

Animals. The Slc17a7-IRES2-Cre (Vgut1-Cre) mouse line was obtained from The Jackson Laboratory (023527). Details for the construction of this mouse were described previously (Harris et al., 2014). The Ai32 line, which was also from The Jackson Laboratory (024109), possesses the ChR2(H134R)-EYFP transgene in the ROSA26 locus. Expression of the ChR2-(H134R)-EYFP is made Cre dependent by separation of the CAG promoter from the transgene by a loxP-flanked STOP cassette (Madisen et al., 2012). Male Vglut1-Cre mice homozygous for the Cre allele were mated with homozygous Ai32 mice to produce compound heterozygote offspring (Vglut1-ChR2), each bearing a Cre and Ai32 allele. To produce control subjects for some experiments, Vglut1-Cre homozygotes were crossed with the R26-EYFP line (Srinivas et al., 2001) obtained from The Jackson Laboratory (006148), producing compound heterozygous offspring that express EYFP in Vglut1-Cre-positive cells. Nav1.8-ChR2 mice were generated by crossing Nav1.8-Cre (Agarwal et al., 2004) with Ai32 mice. Npy2r-ChR2 mice were generated by crossing homozygous Npy2r-IRES-Cre males (Chang et al., 2015), which were obtained from The Jackson Laboratory (029285), with homozygous Ai32 females.

Spared nerve injury (SNI). The SNI model was performed as described previously (Bourquin et al., 2006). Briefly, mice were anesthetized under 2% isoflurane. An incision was made near the lower thigh region and the tibial, common peroneal, and sural nerves were exposed. The tibial and common peroneal nerves were transected using small Iris scissors. Care was taken to avoid touching or stretching the sural nerve. The muscle was closely approximated and the skin incision was closed using 9 mm wound clips (Fine Science Tools). Animals were returned to their home cages after surgery and monitored.

Intraplantar injections. Ropivacaine (0.5%, 20 μl) was injected subcutaneously into the ventral left hindpaw using a 29 g insulin syringe. Care was taken to avoid bleeding. A mixture of QX-314 (Sigma-Aldrich, 552233) and flagellin (Invivogen) was prepared to a final concentration of 60 mM QX-314 and 1 μg of flagellin in sterile PBS, as described previously (Xu et al., 2015). Sterile PBS was used as vehicle. Twenty microliters of each solution was injected intraplantarly in a randomized and blinded fashion (by A.C.).

Behavior. Animals mice (1–4 months of age) of both sexes were used in this study. Mice were housed in the animal care facilities of Duke University School of Medicine. Animals were kept on a 12 h light/dark cycle. All the animal procedures were approved by the Institutional Animal Care and Use Committee of Duke University. Animal experiments were conducted in accordance with the NIH Guide for the Care and Use of Laboratory Animals.

Animals were habituated to the behavior testing room for at least two days before testing commenced. On each day of habituation, and on testing days, mice were placed in individual, cylindrical Plexiglas containers (2.75" ID, 3" Height) with a mesh floor (1/4" × 1/4" in) and allowed to habituate for at least 2 h. Behavioral testing occurred between 11AM - 6PM.

Mechanical threshold. Mechanical thresholds were assayed using calibrated von Frey filaments (North Coast Medical) and the Simplified Up-Down Method (SUDO) (Bonin et al., 2014). Fibers were applied to the sural territory of the hindpaw. Thresholds were determined first for the ipsilateral paw (left) for all mice, and then the contralateral (right) for all mice.

Optogenetic stimulation. A 470 nm LED (Thor Labs, M470F3) was coupled to a 1000 μm fiber (Prizmatix) and an LED driver (D2200, Thor Labs) was used to control the stimulus parameters. For all experiments, 5 ms pulse widths were used. Frequency was varied between 2 and 10 Hz, as indicated. Light intensity was varied between 1 and 10 mW/mm^2 as indicated in each experiment. Light intensity was measured at the tip using a power meter (PM100D, Thor Labs) All behavior was recorded for later analysis using a smartphone camera (iPhone 6S) at 30 frames/s. For plantar photostimulation, the LED-coupled fiber was brought into close proximity (1–2 mm) of the plantar hindpaw but without touching. Stimulation was carried out for 10 s, which was counted as a trial. For behavior shown in Figure 6, for each mouse, 3 trials per mouse were performed, alternating between paws, with at least 2 min between trials. Frequency was increased sequentially from 2 to 5 Hz and then 10 Hz. At each frequency, the intensity was also varied at 1, 2.5, 5, and 10 mW/mm^2. For the experiment shown in Figure 7, 2 Hz was used for all intensities to accurately measure single events. For the experiment depicted in Figure 8, 5 mW/mm^2 and 10 Hz was used. For the experiment depicted in Figures 9 and 10, 10 mW/mm^2, 10 Hz was used. We selected this stimulation setting because it most reliably produced light-evoked behaviors.

Behavior scoring and analysis. Behaviors were scored from recorded videos using either an iPhone 6S or a Logitech HD Pro Webcam C920 acquired at the time of testing. Behavioral coding was conducted using the open source event-logging software BORIS (Friard and Gamba, 2016). The following ethogram was used:

- Lift: Rapid up and down movement,
- Hold: Paw pulled upward toward the bottom and held,
- Flutter: Rapid, repeated lifts in succession,
- Jump: Both hindpaws come off the floor,
- Lick: Paw moved to the mouth and licked,
- Guard: Paw lifted and held laterally and at mid-body level,
- Vocalization: Audible sound such as a squeak, and
- Rear: Mouse extends body vertically and stands on hind legs with support of enclosure.

For the A-fiber blockade experiment depicted in Figure 8, *B* and *C*, and the SNI experiments depicted in Figure 10, both the tester (A.C.) and the scorer (M.M.) were blinded to treatment.

Behaviors were classified as reflexive or affective–motivational in accordance with the definitions in Corder et al. (2017) as follows. Withdrawal reflexes: rapid reflexive retraction of the paw that occurs in response to nociceptive sensory information but ceases once the stimulus is removed and afferent nociceptive information stops; affective–motivational responses: temporally delayed (relative to the noxious stimulus contact or removal of said stimulus), directed licking and biting of the paw (termed "attending"), extended lifting or guarding of the paw and/or escape responses characterized by hyperlocomotion, rearing or jumping away from the noxious stimulus.

In this study, we classified lifting, holding, and flutter as withdrawal reflexes and licking, vocalization, rearing, jumping, and guarding as affective–motivational responses.

Exported data from BORIS was further analyzed in R (http://www.R-project.org/). Plotting and statistical analysis were performed using the following packages: tidyverse, cowplot, readxl, colorblindr, viridis, lme, and lsmeans.

Real-time place escape avoidance. A custom two-chamber apparatus was fashioned with each chamber having dimensions of 10 × 10 × 15 cm and white, opaque walls. A 5 × 4 cm hole was made at the midpoint of the wall joining the two chambers. Horizontal black striped walls were pres-

ent in one chamber and vertical stripes in the other to provide visually distinct cues for each chamber. The two-chamber apparatus was positioned on top of the same mesh floor used for other behavior experiments. A camera (Logitech HD Pro Webcam C90) was positioned above the chambers. Real-time automated video tracking was performed by a connected PC (Dell) running the ANY-MAZE tracking software (Stoelting).

A mouse was introduced into one of the two chambers at random. Mice were first allowed to freely explore two chambers for 10 min (prestimulation). During this prestimulation period, the majority of mice exhibited a preference for one or the other chamber. The chamber in which each mouse spent the majority of the prestimulation period was taken as its preferred chamber. Immediately following the prestimulation period, the stimulation period began, during which time each mouse was allowed to move freely between chambers. Whenever the mouse was in its preferred chamber, blue light (470 nm, 10 mW/mm^2, 10 Hz) was applied to a single hindpaw (left), and whenever the mouse was in its nonpreferred chamber, off-spectrum, yellow light (565 nm) was applied to the hindpaw with a fiber-coupled LED (Thor Labs, M565F1) 10 mW/mm^2 to control for the presence of an experimenter and visual stimulation from light application. After the 10 min stimulation period, light application ceased and the mice were allowed to move freely between chambers during a 10 min poststimulation period. For the real-time place escape/avoidance (RT-PEA) assay depicted in Figure 10, mice were stimulated with blue light on the ipsilateral (left) paw when in the preferred chamber and on the contralateral paw when in the nonpreferred chamber, analogous to the traditional RT-PEA assay performed with von Frey fibers (Pratt et al., 2013).

Immunohistochemistry and in situ *hybridization.* Animals were deeply anesthetized with isoflurane and transcardially perfused with 4% paraformaldehyde. After perfusion, lumbar DRG (L3–L5) and spinal cord were removed and postfixed in the same fixative for 2 h at 4°C. Then, the tissues were cryopreserved in 30% sucrose/PBS solution for at least 24 h. All tissues were mounted in optimal cutting temperature (OCT) medium (Tissue-Tek) or PBS (free-floating sections) and cryosectioned using a cryostat (Leica). For immunofluorescence and *in situ* hybridization, DRG sections were cut at 12 μm and thaw-mounted onto Superfrost Plus slides (VWR), and spinal cord sections were cut at 14 μm and thaw-mounted.

For immunostaining of DRG, sections were blocked in a solution containing 1% BSA and 0.4% Triton X-100 for 1 h at room temperature (RT). After blocking, the sections were incubated overnight with primary antibodies diluted in 1% BSA with 0.2% Triton X-100 at 4°C. After washing 3 times in PBS for 5 min at RT, sections were incubated with the appropriate secondary antibody for 1 h at RT followed by 3 washes in PBS for 5 min. Before mounting, some sections were counterstained with DAPI and fluorescent Nissl stain (NeuroTrace 640/660, Thermo Fisher Scientific). Slides were then mounted in Prolong Gold (Life Technologies) and allowed to dry overnight at room temperature.

In situ hybridization was performed using the RNAscope system (Advanced Cell Diagnostics) according to the manufacturer's recommendations. Tissue pretreatment for DRG sections consisted of incubation with protease IV for 30 min at room temperature. Subsequently, the protocol for the Multiplex Fluorescent Kit version 2 was followed without modification until the final wash step, after which immunostaining with anti-GFP antibody was performed. Combing immunostaining with RNAscope was necessary to recover the ChR2-EYFP signal because the protease treatment abolishes the native EYFP fluorescence. The probes used were Slc17a7 (Mm-Slc17a7, 416631), Ret (Mm-Ret, 431791), Tlr5 (Mm-Tlr5, 451601), Ntrk2 (Mm-Ntrk2-C2, 423611-C2), and Nefh (Mm-Nefh-C3, 443671-C3).

Skin immunostaining was performed as in as described by Arcourt et al., 2017. Briefly, skin from the hindpaw was fixed in methanol/acetone (1:1) for 30 min at −20°C, washed 4 times with PBS, and then incubated in 30% sucrose for at least 24 h at 4°C. After embedding in OCT, 50 μm cryosections were cut, dried, incubated in 50 mM glycine for 45 min, washed twice with PBST (0.2%), blocked for 1 h with blocking buffer (0.2% PBST, 10% horse serum,1% BSA), and then incubated with primary antibodies overnight at 4°C. After primary staining, sections were washed 3 times, incubated with secondary antibody at room temperature for 1 h, washed another 3 times, counterstained with DAPI, and then mounted with Prolong Gold.

Primary antibodies were used at the following dilutions: mouse anti-NF200 (1:500, Sigma-Aldrich, N0142, RRID:AB_477257), chicken anti-GFP (1:1000, Abcam, 13970, RRID:AB_300798), anti-CGRP (1:1000, Sigma-Aldrich C8198, RRID:AB_259091), rabbit anti-TH (1:1000, Millipore AB152, RRID:AB_390204), TROMA-1 (Iowa Developmental Studies Hybridoma Bank, 1:200). Secondary antibodies were as follows: Cy3-conjugated anti-rabbit IgG (1:500, Jackson ImmunoResearch), Alexa Fluor 488-conjugated anti-Chicken IgG (1:500, Jackson ImmunoResearch), Alexa Fluor 546-conjugated anti-Chicken IgG (1:500, Thermo Fisher Scientific), Cy3-conjugated anti-Mouse IgG (1:500, Jackson ImmunoResearch). For some sections, Alexa Fluor 568–Isolectin GS-IB4 from *Griffonia simplicifolia* (Thermo Fisher Scientific) was used at a 1:1000 dilution during secondary antibody incubation.

Image analysis. Imaging was performed using an epifluorescence microscope (Nikon Eclipse NiE). For quantification, all images were taken using the same acquisition settings. For DRG quantitation, every fifth section was counted, with two to four DRG sections from each animal. Images in Figure 1 were analyzed in Adobe Photoshop CC. For each staining combination, a threshold was set and globally applied for each color channel and coexpression events were counted manually. For ISH experiments in Figure 2, we used the bioimage analysis software QuPath (Bankhead et al., 2017). Borders were drawn manually around cells to define regions of interest. The cross-sectional area and mean intensity for each color channel were extracted for each cell. A histogram of the mean intensities for each channel was plotted in R. For ChR2-EYFP a clear bimodal distribution was apparent and the boundary between the population was used to classify cells as positive or negative. For *Ret* and *Nefh*, a continuous distribution was apparent. To set a threshold for each channel, we sampled cells in QuPath that were judged to be completely negative of signal and set a threshold of 1 SD above the mean of the negative cells. Cells above the threshold were considered positive. The areas of the cells from this set were used to determine the proportion of ChR2-EYFP cells comprising each size class in Figure 1*D*. *Tlr5* was expressed more sparsely and presented as puncta rather than filling the whole cell. Thus, we used instead the "subcellular detection" analysis feature of QuPath to count individual spots. A spot threshold was set and cells with spot counts above the threshold were classified as positive.

Patch-clamp recordings in dissociated DRG neurons. DRGs were aseptically removed from mice (5–6 weeks old) and digested with collagenase type II (0.2 mg/mL Roche) and Dispase II (3 mg/mL Worthington) for 120 min. Cells were seeded onto poly-D-lysine-coated glass coverslips and incubated for 16–48 h in Neurobasal medium (10% FBS, 2% B27, and 1% antibiotic–antimycotic) at 37°C with 5% CO_2 before the experiment. Whole-cell voltage-clamp recordings were performed at room temperature with an EPC10 amplifier (HEKA). Pipettes were pulled from borosilicate glass to a resistance of 2–5 MΩ. The bath solution consisted of the following (in mM): 140 NaCl, 3 KCl, 2 $MgCl_2$, 2 CaCl2, 10 glucose, and 10 HEPES. The internal pipette solution consisted of the following (in mM): 5 NaCl, 130 K-gluconate, 2 MgCl2, 10 EGTA, and 10 HEPES. Optical stimulations were performed using 470 nm light delivered from a 40× objective (Olympus). The light source was white light (CoolLED pE-300) filtered with a GFP Fluorecence Cube Set (470/525 Em/Ex) at 10% maximum intensity. Series resistance was compensated at least 60% and only cells for which the resistance remained stable and below MΩ were used for subsequent analysis. Liquid junction potential, calculated using the JPCalc software, was corrected *post hoc*. Analysis of the spike success rate was performed following a 5 s optogenetic stimulation at 5 or 10 Hz. This was repeated 5 times per cell with 10 s in between stimulus bouts. The corresponding activity was binned at the appropriate period associated with the stimulus frequency and the mean success rate was calculated as a function of pulse number across cells. The shaded regions in Fig. 5*C–D* are the SEM.

Experimental design and statistical analyses. Behavioral tests were conducted in a blinded fashion both during data acquisition and scoring, with the exception of the experiments presented in Figures 6 and 7, in which the tester (A.C.) was aware of the identity of the subjects. However,

the scorers (M.M. and B.T.) were blinded to the identity of the subjects during scoring. Scoring of behavioral data was performed in a blinded fashion after data acquisition using the open source behavioral coding software BORIS or automatically by video analysis (RT-PEA). Imaging data acquisition was performed by an investigator with knowledge of the identity of the experimental groups (M.W., A.C., or M.M.). Statistical tests for behavioral experiments in which subjects were repeatedly measured consisted of factorial linear mixed effects (LME) models with subject as a random effect. Test results for each behavioral experiment are indicated in the figure captions. Statistical tests were conducted in R. Group sizes for behavioral, imaging, and electrophysiological experiments were based on previous such experiments in our laboratory.

Results

Distribution of ChR2-EYFP in the DRG

To gain genetic access to A β-LTMRs, we crossed a Vglut1-Cre transgenic mouse line (Slc17a7-IRES2-Cre) (Harris et al., 2014) to a Cre-dependent ChR2-EYFP reporter line (Ai32) (Madisen et al., 2010) because it has been demonstrated that Vglut1 is expressed preferentially in low-threshold mechanoreceptors (Alvarez et al., 2004; Brumovsky et al., 2007), in contrast to *Vglut2* and *Vglut3*, which are expressed preferentially by nociceptors and C-fiber LTMRs, respectively(Rogoz et al., 2012). We refer to the offspring of this cross as Vglut1-ChR2.

To examine the distribution of ChR2-EYFP and coexpression with canonical class markers, we performed immunohistochemical staining and *in situ hybridization* on lumbar DRGs of Vglut1-ChR2 mice (Fig. 1*A–C*). Fourteen percent (248/1667) of all DRG neurons (Nissl stain) expressed ChR2-EYFP; 95% (487/505) of ChR2-EYFP-positive neurons in Vglut1-ChR2 mice coexpressed *Vglut1* mRNA by *in situ* hybridization, whereas 59% (487/830) of *Vglut1*-positive neurons coexpressed ChR2-EYFP, demonstrating that ChR2-EYFP expression is highly specific but incompletely penetrant.

Seventy-eight percent (228/296 neurons) of ChR2-EYFP-positive neurons coexpressed NF200, a marker of myelinated fibers (Berta et al., 2017). Conversely, 42% (228/561) of NF200-positive neurons coexpressed ChR2-EYFP. ChR2-EYFP-positive neurons showed negligible coexpression with isolectin-B4 (IB4, 3%, 10/351) and calcitonin gene-related peptide (CGRP, 5%, 13/263), markers of nonpeptidergic and peptidergic nociceptors, respectively (da Silva Serra et al., 2016). Coexpression of ChR2-EYFP-positive neurons with tyrosine hydroxylase (TH), a marker of low-threshold, unmyelinated C-LTMRs (Draxler et al., 2014), was virtually undetectable (2%, 5/229 neurons). Overall, the mean cross-sectional area of ChR2-EYFP-positive neurons ($786 \pm 20\ \mu m^2$, $n = 248$) was substantially larger than that of all DRG neurons ($368 \pm 6\ \mu m^2$, $n = 1667$) (Fig. 1*D*). Consistently, we also found that ChR2-EYFP-positive neurons constituted more than half of all large-sized neurons ($>600\ \mu m^2$) (Fig. 1*E*). Taken together, these results indicate that vast majority of ChR2-EYFP-positive cells in Vglut1-ChR2 mice are myelinated, medium- to large-sized neurons that express *Vglut1* and are not nociceptors or C-LTMRs.

To further characterize the identities of Vglut1-ChR2 neurons, we used *in situ* hybridization to determine the coexpression of ChR2-EYFP with more specific markers of Aβ-LTMRs, *Ret* and Toll-like receptor 5 (*Tlr5*) (Fig. 2*A*,*B*). *Ret* is a marker for rapidly adapting Aβ-LTMRS (RA-Aβ-LTMRs) (Luo et al., 2009), Aβ-field LTMRs (Bai et al., 2015), as well as nonpeptidergic C-nociceptors. To distinguish between LTMRs and C-nociceptors, we used the combination of *Ret* with *Nefh* (i.e., mRNA for NF200) to identify *Ret*-expressing Aβ-LTMRs. *Tlr5* is expressed broadly by Aβ-LTMRs but not other types of PSN (Xu et al., 2015). A large portion of the ChR2-EYFP-positive population (35%, 180/532) coexpressed the combination of *Ret*/*Nefh*, indicating that these are either RA-Aβ- or field-LTMRs. A comparable fraction of all *Ret*/*Nefh* neurons (41%, 180/428) coexpressed ChR2-EYFP (Fig. 2*C*,*D*). More than half of all ChR2-EYFP-positive neurons coexpressed *Tlr5* (66%, 340/541) and 42% (340/800) of *Tlr5*-positive neurons coexpressed ChR2-EYFP (Fig. 2*E*), further corroborating the identification of these neurons as Aβ-LTMRs. Additionally, we examined the expression of *TrkB* by ISH, as this gene is known to mark RA-Aβ-LTMRs and Aβ-LTMRs (Bourane et al., 2009). Interestingly, we found that most neurons expressing high levels of *TrkB* do not coexpress ChR2-EYFP, but some ChR2-EYFP do express low levels of *TrkB*, as do satellite glia (Fig. 3).

Spinal and cutaneous projections of Vglut1-ChR2 DRG neurons

In the spinal cord, ChR2-EYFP-positive afferent fibers were evident in the deep dorsal horn (lamina III–V), the dorsal columns (DCs) and, to a lesser extent, the ventral horn (Fig. 4*A*). ChR2-EYFP-positive fibers were not present in the superficial laminae (I–IIi), where most nociceptive inputs are processed (Basbaum et al., 2009), as evidenced by the lack of overlap with CGRP-positive or IB4-positive afferents. The absence of ChR2-EYFP-positive fibers in the superficial dorsal horn suggests that they are not C- or Aδ-nociceptors. The high density of ChR2-EYFP-positive afferents in the deep laminae and dorsal columns supports the identification of the remainder of the afferents in this region as Aβ-LTMRs. The presence of ChR2-EYFP-positive fibers in the ventral horn also indicates that some ChR2-EYFP-positive neurons are proprioceptors, consistent with previous findings regarding Vglut1 expression in the spinal cord (Todd et al., 2003).

In the skin, ChR2-EYFP-positive afferents were present in the dermis and formed characteristic cutaneous end organs. In the glabrous skin of the hindpaw, ChR2-EYFP-positive fibers were present in close contact with TROMA1-positive Merkel cells in Merkel cell–neurite complexes (Fig. 4*B*, top), and also in Meissner corpuscles in the dermal papillae(Fig. 4*B*, middle), which are features of slowly adapting (SA)-Aβ-LTMRs and RA-Aβ-LTMRs, respectively (Abraira and Ginty, 2013). In the hairy skin of the hindpaw, ChR2-EYFP-positive fibers were also found encircling hair follicles in longitudinal lanceolate endings. These findings demonstrate that the population of cutaneous ChR2-EYFP-positive fibers represents at least two distinct subtypes of Aβ-LTMR.

Electrophysiological characterization of Vglut1-ChR2 DRG neurons

Patch-clamp recording was performed on dissociated DRG neurons from *Vglut1-ChR2* mice *in vitro*. The majority of ChR2-YFP-positive neurons (6/7) responded with only a single or a few spikes after receiving constant photostimulation (1 s), followed by a prolonged depolarization above baseline that was absent in ChR2-EYFP-negative controls (Fig. 5*A*,*H*). The majority of ChR2-EYFP-positive DRG neurons faithfully produced action potentials up to a stimulus frequency of 10 Hz, whereas ChR2-EYFP-negative DRG neurons did not. This suggests the neuronal activity was entrained to the stimulus specifically in the subset of DRG neurons expressing ChR2-EYFP (Fig. 5*B–D*). ChR2-EYFP-positive DRG neurons all lacked an inflection in the repolarization phase often found in ChR2-EYFP-negative neurons (Fig. 5*E*). Further characterization of the spike waveform revealed that the action potential half-width of ChR2-EYFP-positive DRG neurons was significantly lower than that of ChR2-EYFP-

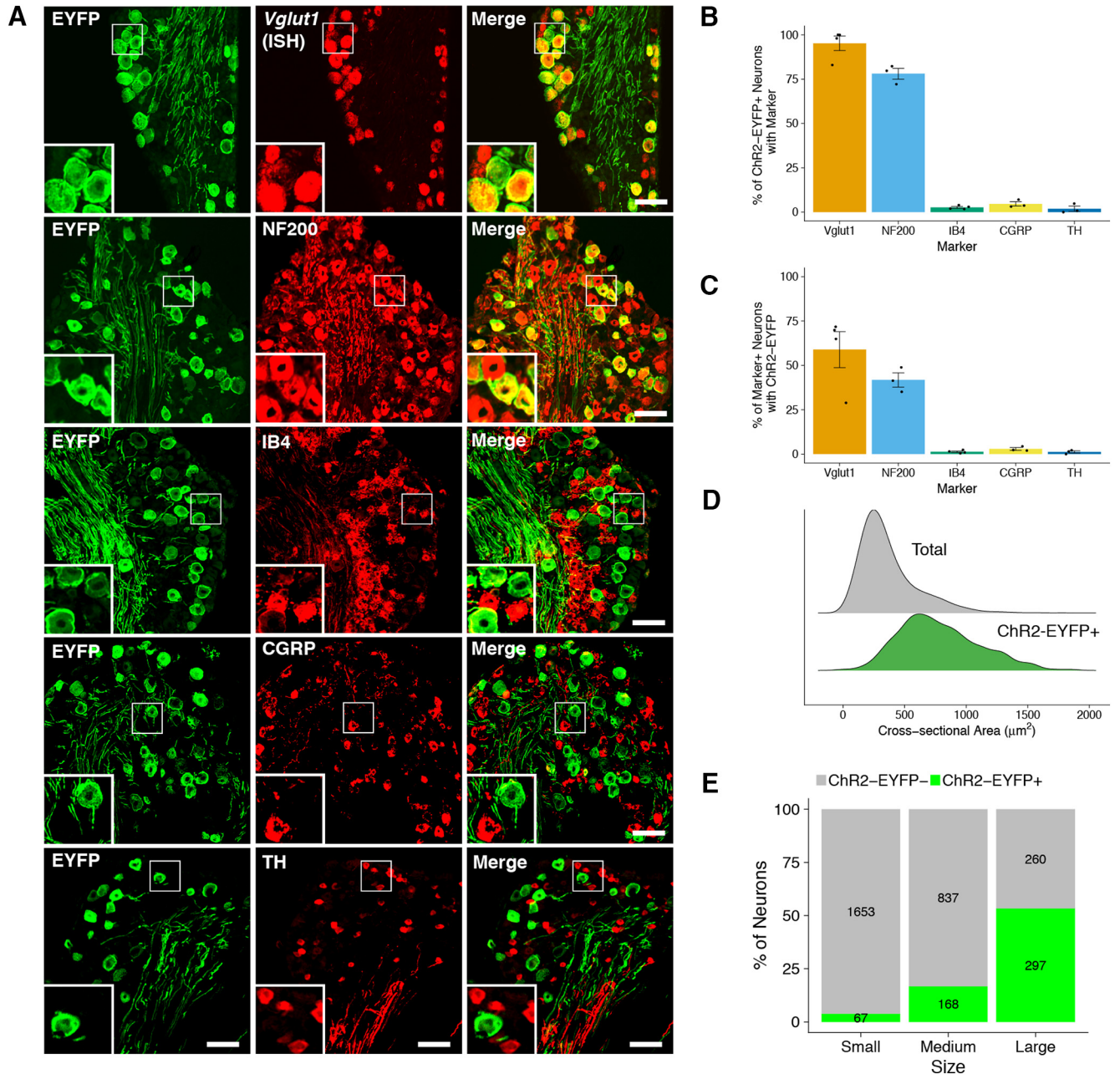

Figure 1. Cellular distribution of ChR2-EYFP in dorsal root ganglia. ***A***, ChR2-EYFP coexpression with selected markers in DRG. Scale bar, 50 μm. ***B***, ***C***, Quantification of coexpression of ChR2-EYFP with selected markers (mean ± SEM, $n = 4$ animals, 3–4 sections/animal). ***D***, Size distribution of all (total) and ChR2-EYFP-positive DRG neurons expressed as probability density. ***E***, Proportion of ChR2-EYFP-positive neurons in each size class of DRG neuron. Small: <300 μm; medium, 300 – 600 μm; large, >600 μm. Values inside bars represent the number of ChR2-EYFP-positive (green) and ChR2-EYFP-negative (gray) neurons in each size class ($n = 6$ animals, 2–3 sections/animal).

negative neurons (Fig. 5*F*). Both of these properties are consistent with those of LTMRs (Smith and Lewin 2009). Spike thresholds were also found to be significantly lower in ChR2-EYFP-positive DRG compared with ChR2-EYFP-negative neurons (Fig. 5*E*).

Light-evoked withdrawal behaviors in naive Vglut1-ChR2 mice

We applied blue light (470 nm) to the plantar surface of the hindpaw to assess the behavioral response to activation of Vglut1-ChR2 neurons. We measured several facets of the behavioral response. We took paw withdrawal as a primary measure, but we also measured secondary behaviors that reflect the nature of the withdrawal. We classified behaviors as "reflexive" (lift, hold, jump, flutter) and others as "affective–motivational" (guard, lick, rear, vocalize) in accordance with the paradigm described in Corder et al. (2017). A full description of the scoring paradigm can be found in the Materials Methods. We also scanned a range of light intensities (1–10 mW/mm^2) and frequencies (2–10 Hz) consistent with the parameters used in similar studies of optogenetic stimulation of primary sensory neurons (Arcourt et al., 2017).

The typical response to photostimulation of the hindpaw was a rapid paw lift or no response, depending on the stimulation parameters. Response frequency, which measures whether the mouse responded at all during a 10 s trial, increased with both

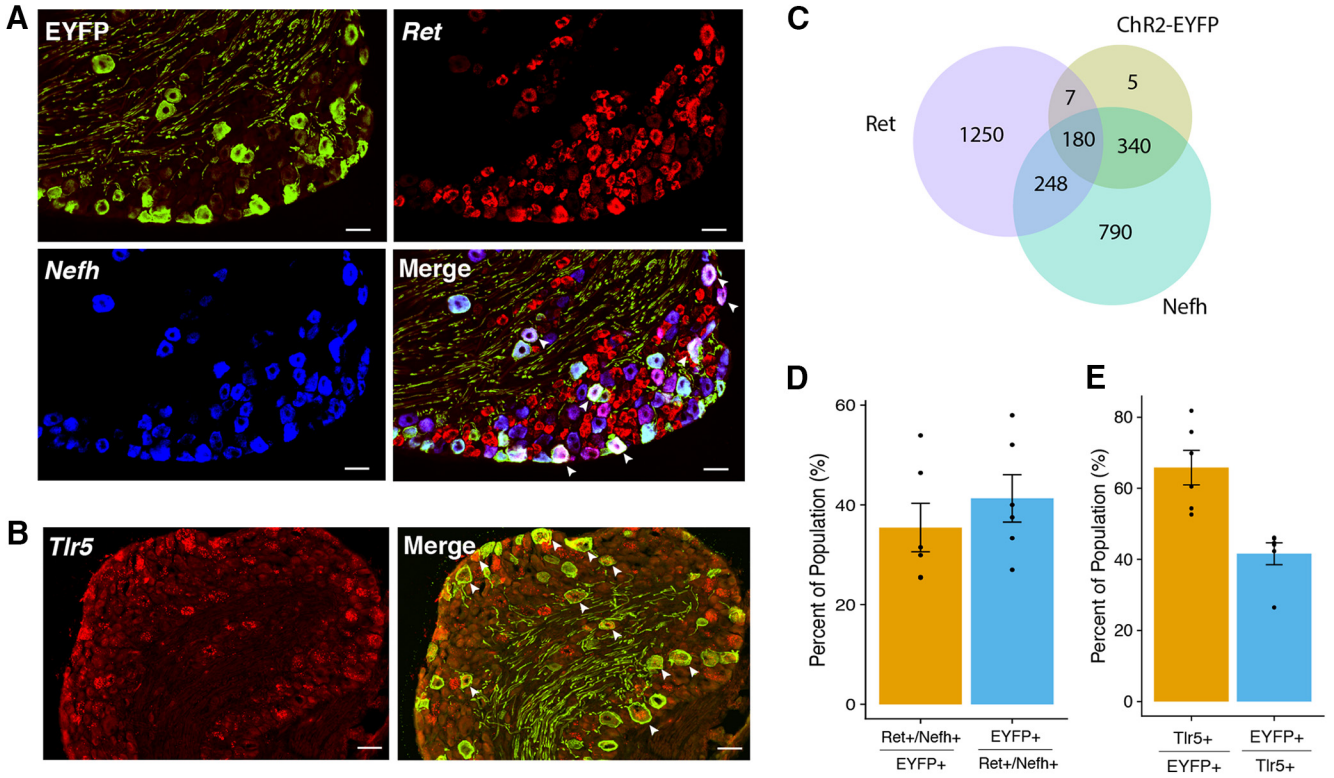

Figure 2. Coexpression with Aβ-LTMR markers. ***A***, ***B***, Coexpression of ChR2-EYFP with Nefh and Ret (***A***) and Tlr5 (***B***). Scale bar, 50 μm. Arrows indicate cells that coexpress all markers. ***C***, Venn diagram of ChR2-EYFP, Nefh, and Ret. ***D***, ***E***, Quantification of coexpression for ChR2-EYFP, Nefh, and Ret represented as a percentage of the population (mean ± SEM, $n = 6$ animals, 2–3 sections/animal).

light intensity and frequency (Fig. 6*A*), reaching a maximum at 10 mW/mm^2. The total number of events per trial also increased with increasing intensity and frequency (Fig. 6*B*). At all intensities and frequencies, the most frequently observed behavior was lifting (Fig. 6*C*). Affective–motivational behaviors were scarcely seen, even at the highest intensities and frequencies, whereas reflexive behaviors increased up to 10 mW/mm^2 (Fig. 6*D*,*E*).

To better understand the nature of the light-evoked responses in Vglut1-ChR2 mice, we directly compared paw withdrawal behaviors in Vglut1-ChR2 mice with those of Nav1.8-ChR2 mice, a line that conditionally expresses ChR2 in the majority of nociceptors and has been thoroughly characterized previously (Daou et al., 2013) . For this comparison, we used low frequency (2 Hz) so that we could accurately measure individual events. The response frequency of Nav1.8-ChR2 was significantly greater than that of Vglut1-ChR2 at 1 and 2.5 mW/mm^2 (Fig. 7*A*). The number of behavioral responses per trial was markedly different between the two mouse lines; Nav1.8-ChR2 mice responded to light many more times during a 10 s trial than did Vglut1-ChR2 mice at every intensity (Fig. 7*B*). In contrast to Vglut1-ChR2 mice, Nav1.8-ChR2 displayed many more stereotypical nocifensive behaviors including licking, jumping, and vocalization as intensity increased (Fig. 7*C*,*D*). Some pain-related behaviors, such as audible vocalizations (Williams et al., 2008), which were never observed in Vglut1-ChR2 mice, appeared prominently at 10 mW/mm^2 in Nav1.8-ChR2 mice. However, even for Nav1.8-ChR2 mice, the most numerous type of response was reflexive (Fig. 7*E*). Taken together, these results indicate that the behavioral responses elicited by photostimulation of cutaneous Vglut1-ChR2 neurons are likely non-nociceptive given their marked divergence from the behaviors elicited by the same stimuli in Nav1.8-ChR2 mice.

Local anesthetic and A-fiber selective blockade abolishes light-evoked paw withdrawal

To confirm that light-evoked withdrawal behaviors in Vglut1-ChR2 mice required neuronal firing, we injected the sodium channel-blocking local anesthetic ropivacaine (0.5%) subcutaneously in one hindpaw and then photostimulated both the ipsilateral and contralateral paws 30 min after injection at 10 mW/mm^2 and 10 Hz. Ipsilateral photostimulation resulted in only 10% of mice responding (1/9), but 100% responding on the contralateral side (9/9), thus confirming that light-evoked withdrawal in Vglut1-ChR2 requires neuronal action potential firing (Fig. 8*A*). To determine more precisely whether light-evoked withdrawal behaviors in Vglut1-ChR2 were due to neuronal activity of A-fibers, we used a combination of the TLR5 ligand flagellin and the membrane-impermeable sodium channel blocker QX-314, as we recently demonstrated that this mixture produces selective and reversible A-fiber blockade (Xu et al., 2015) . Because the majority (~60%) of Vglut1-ChR2 neurons express *Tlr5* (Fig. 2*B*,*E*), we predicted that this pharmacological blockade would attenuate light-evoked behaviors upon plantar photostimulation. Indeed, response frequency and number of events per trial were dramatically reduced in the ipsilateral paw 30 min after intraplantar injection of flagellin/QX-314 (1 μg/60 mM) but not vehicle (PBS) control (Fig. 8*B*,*C*). Contralateral photostimulation did not differ between the treatment groups, corroborating the specificity of A-fiber blockade.

Activation of cutaneous Vglut1-ChR2 neurons is not aversive

To assess whether activation of Vglut1-ChR2-positive neurons is aversive, we adapted a two-chamber, RT-PEA assay that was recently used to test aversion caused by optogenetic activation of

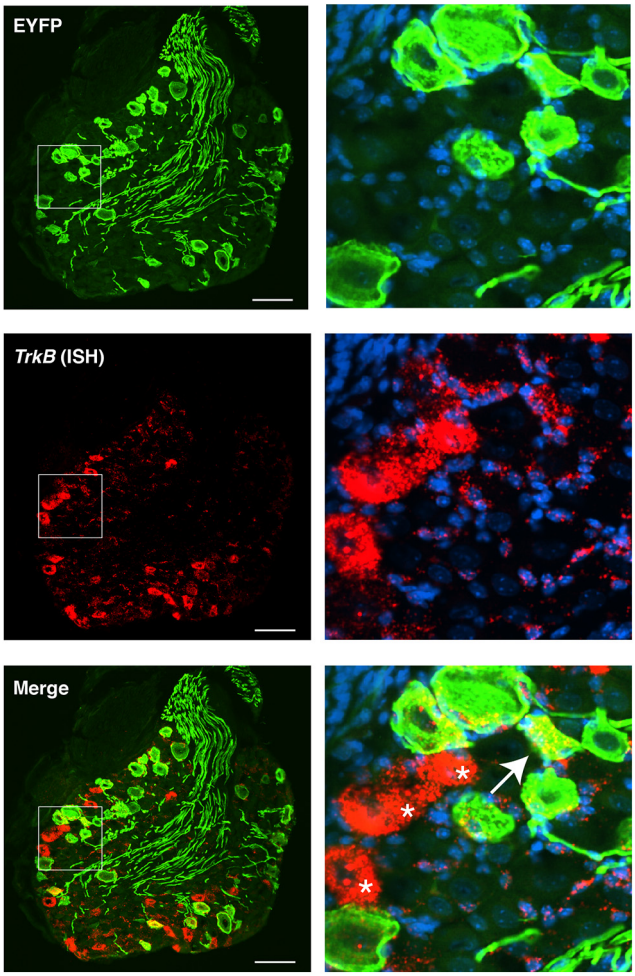

Figure 3. Expression of TrkB in Vglut1-Chr2 DRG. Left, Coexpression of ChR2-EYFP transcript by ISH. Arrow indicates a ChR2-EYFP-positive neuron coexpressing low levels of TrkB. Asterisk indicates highly expressing TrkB-positive neurons that lack ChR2-EYFP expression, which are likely Aδ-LTMRs. Note the expression of TrkB around the circumference of ChR2-EYFP-positive neurons, likely in satellite glia cells. Scale bar, 50 μm. Right, Magnification of inset.

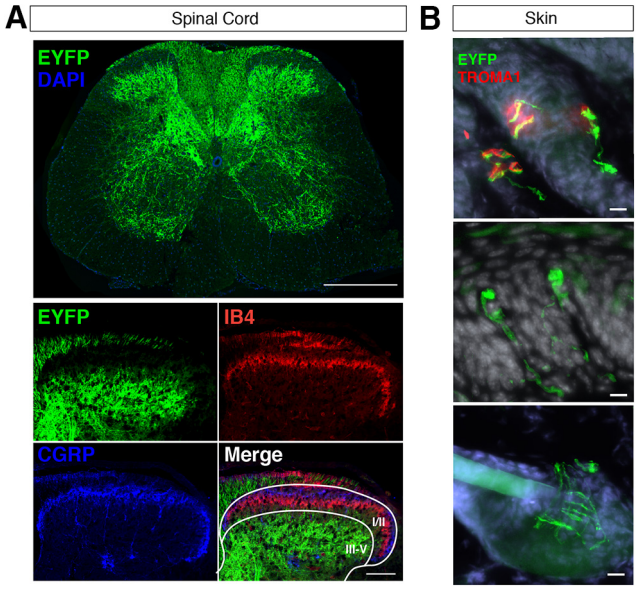

Figure 4. Spinal and cutaneous projections of ChR2-EYFP-positive neurons in Vglut1-ChR2. ***A***, Low magnification of ChR2-EYFP-positive afferents in the lumbar spinal cord (top). Scale bar, 500 μm. High-magnification images of ChR2-EYFP-positive, CGRP-positive, and IB4-positive afferents in the dorsal horn (bottom). Scale bar, 100 μm. Laminar borders (white) are represented in the merged image. ***B***, Cutaneous projections of ChR2-EYFP-positive afferents in glabrous (top and middle) and hairy (bottom) skin. In the top panel, ChR2-EYFP-positive afferents make direct contacts with TROMA1-positive (red) Merkel cells in glabrous skin. Scale bar, 10 μm.

TRPV1-ChR2-positive nociceptors in the trigeminal system (Rodriguez et al., 2017) (Fig. 9*A*). We performed this RT-PEA assay on Vglut1-ChR2 mice as well as Vglut1-EYFP control animals. Consistent with our other results supporting a non-nociceptive character of Vglut1-ChR2-positive neurons, blue light photostimulation of the plantar hindpaw did not produce statistically significant aversion during the stimulation period or the poststimulation period in Vglut1-ChR2 mice and Vglut1-EYFP controls (Fig. 9*B*,*E*,*F*). By contrast, Nav1.8-ChR2 mice showed strong aversion during the stimulation period that persisted into the poststimulation period as well, demonstrating that this RT-PEA assay can report on the aversiveness of an experience if the stimulus is adequate (Fig. 9*B*,*E*,*F*).

Because the Nav1.8-ChR2-positive population makes up a large proportion of all DRG neurons, it is possible that the observed differences in aversion behavior between Vglut1-ChR2 and Nav1.8-ChR2 mice were a consequence of the number of neurons activated rather than the distinct characteristics of the two populations. To address this possibility, we generated an additional mouse line in which ChR2 is conditionally expressed in neuropeptide receptor Y receptor 2 (*Npy2r*)-positive A-mechanociceptors. Npy2r-ChR2-positive neurons make up a much smaller proportion of all DRG neurons than Nav1.8-ChR2 neurons and thus are more comparable to the Vglut1-ChR2-positive population with respect to number of neurons that would receive photostimulation at the hindpaw (Arcourt et al., 2017) . In the RT-PEA assay, Npy2r-ChR2 mice showed strong aversion during the stimulation period and poststimulation period, comparable to that seen in Nav1.8-ChR2 mice (Fig. 9*C*,*E*,*F*). Collectively, these findings indicate that optogenetic activation of Vglut1-ChR2-positive LTMRs does not produce aversion, whereas activation of both large and small populations of nociceptors does produce strong aversion. Furthermore, these results suggest that it is type rather than number of sensory neurons activated that determines the aversiveness of a stimulus.

Optogenetic stimulation of Vglut1-ChR2 mice in the setting of nerve-injury-induced neuropathy

Having established that cutaneous Vglut1-ChR2-positive neurons are Aβ-LTMRs and that their activation by light neither produces pain-like behaviors nor aversion in naive mice, we next sought to address the principal question of this study: Does activation of Aβ-LTMRs alone elicit nociceptive behaviors under pathological conditions? To that end, we used the SNI on Vglut1-ChR2 mice to induce mechanical hypersensitivity in the sural territory of the hindpaw. To minimize intersubject variation, we used the contralateral paw as a within-subject comparison for the injured hindpaw. To assess mechanical hypersensitivity from a natural mechanical stimulus, we used von Frey monofilaments to determine the 50% paw-withdrawal threshold (PWT). One week after nerve injury, on postoperative day 7 (POD7), the mice showed a marked reduction in PWT in the ipsilateral paw compared with baseline, but not the contralateral paw, consistent with previous studies using the SNI model in mice (Bourquin et al., 2006) (Fig. 10*A*). On POD7 we tested light-evoked behaviors across a range of intensities at constant frequency (10 Hz). We

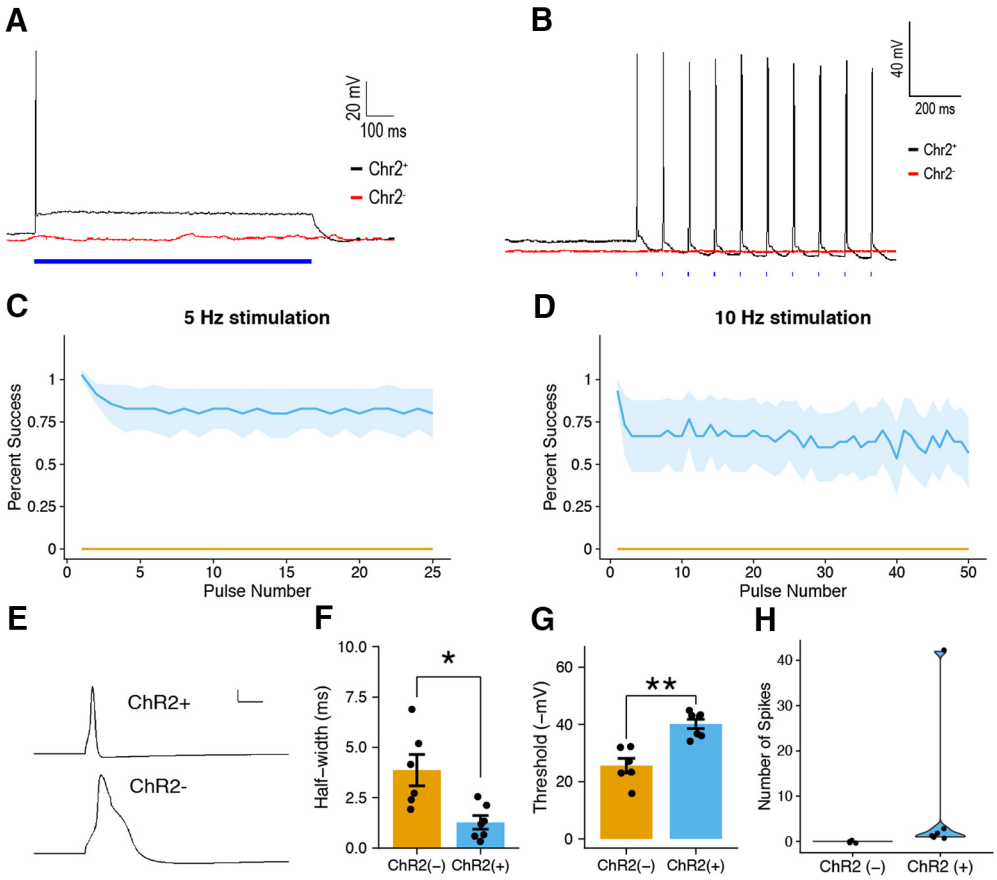

Figure 5. Patch-clamp electrophysiology of ChR2-EYFP-positive and ChR2-EYFP-negative DRG neurons. ***A***, Continuous exposure to 470 nm light for 1 s resulted in depolarization and light-evoked action potentials in ChR2-EYFP-positive DRG neurons (black) but not ChR2-EYFP-negative neurons (red). ***B***, Exposure to light at 10 Hz drove phase-locked action potential firing in ChR2-EYFP-positive DRG neurons (black) but not ChR2-EYFP-negative controls (red). ***C***, ***D***, Success rate at 5 Hz and 10 Hz photostimulation of ChR2-EYFP-positive ($n = 7$) and ChR2-EYFP-negative ($n = 4$) neurons. ***E***, Representative action potential waveforms from ChR2-EYFP-positive (top) and ChR2-EYFP-negative (bottom) DRG neurons. ***F***, Width of the action potential waveform at half-maximum amplitude of ChR2-EYFP-positive and ChR2-EYFP-negative DRG neurons (Student's two-tailed t test, $^*p < 0.05$). ***G***, Action potential threshold of ChR2-EYFP-positive and ChR2-EYFP-negative DRG neurons (Student's two-tailed t test, $^{**}p < 0.005$). ***H***, Number of spikes under continuous photostimulation in ChR2-EYFP positive and ChR2-EYFP-negative neurons. ***C***, ***D***, and ***F***–***H*** are shown as means ± SEM.

did not observe statistically significant differences between the ipsilateral and contralateral paws with regard to the number of any kind of behavior (Fig. 10*B–D*). There was no increase in affective–motivational behaviors (e.g., licking, vocalizing, guarding) in the ipsilateral paw compared with baseline or between paws.

To test relative aversiveness of photostimulation of the injured hindpaw, we subjected the SNI cohort to a modified version of the RT-PEA assay on POD8. In this modified RT-PEA, we applied blue light (10 mW/mm^2, 10 Hz) to the sural territory of the ipsilateral hindpaw when the mouse was in its preferred chamber and to its contralateral paw when in the nonpreferred chamber, analogously to the traditional PEA assay that uses von Frey filaments to assess unilateral insults (Pratt et al., 2013). We did not observe any changes in chamber preference during the stimulation period or the poststimulation period, indicating that activation of Vglut1-ChR2-positive neurons in an injured hindpaw does not produce any relative aversion compared with stimulation of an uninjured hindpaw (Fig. 10*E*,*F*).

Discussion

In this study, we described a novel Vglut1-ChR2 transgenic mouse line and demonstrated its utility as a tool to activate cutaneous Aβ-LTMRs via transdermal optogenetic stimulation. We exploited the Vglut1-ChR2 line to determine whether specific activation of cutaneous Aβ-LTMRs is sufficient to produce pain-like behaviors in the setting of neuropathy, a key outstanding question in pain research. Our findings suggest that activation of Aβ-LTMRs alone does not underlie the allodynia-like mechanical hypersensitivity observed in neuropathic pain models in mice. If true, then this conclusion would warrant a reconsideration of the consensus view that Aβ-LTMRs are the substrate for mechanical allodynia. Although they are intriguing, our findings must be interpreted cautiously and in light of multiple caveats. Several lines of evidence suggest that Aβ-LTMRs do contribute to mechanical allodynia in neuropathic contexts (Xu et al., 2015), so how can we reconcile our findings with the existing body of evidence?

Type and number of LTMRs

First, not all Aβ-LTMRs are accessed in the Vglut1-ChR2 mouse; ~50% of large-sized DRG neurons are not labeled by ChR2-EYFP and thus are not activated by photostimulation. Similarly, the incomplete overlap of ChR2-EYFP with *Vglut1* and *Tlr5* mRNA further corroborates that there are Aβ-LTMRs that are not accessed. Thus, our findings can only be applied to Vglut1-ChR2-positive sensory neurons and not the entire population of Aβ-LTMRs. The remaining Aβ-LTMRs that do not express ChR2-EYFP in the Vglut1-ChR2 mouse may be necessary to effect pain-like behaviors in the setting of injury. Alternatively, it

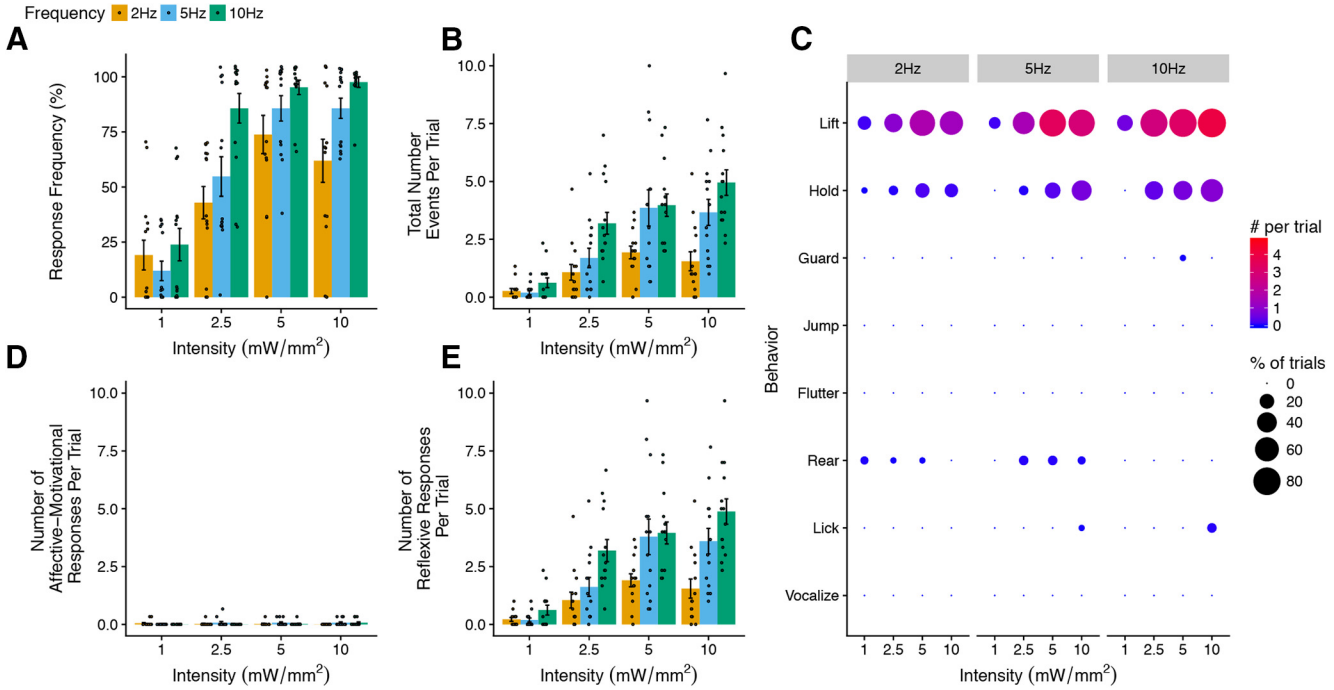

Figure 6. Light-evoked withdrawal behaviors in naive Vglut1-ChR2 mice. ***A***, Response frequency (i.e., the fraction of all trials with at least one response per trial) increases with the intensity and frequency of light stimulation ($n = 14$). ***B***, Total number of all behavioral responses increases with intensity and frequency of light stimulation ($n = 14$). ***C***, Dot plot representation of individual scored behaviors at each intensity and frequency combination. The size of each dot represents the percent of trials in which the behavior was observed, and the color represents the total number of a given behavior per trial, with red indicating higher numbers and blue indicating lower numbers. ***D***, ***E***, Number of affective–motivational and reflexive responses per trial. ***A***, ***B***, ***D***, and ***E*** are shown as means ± SEM.

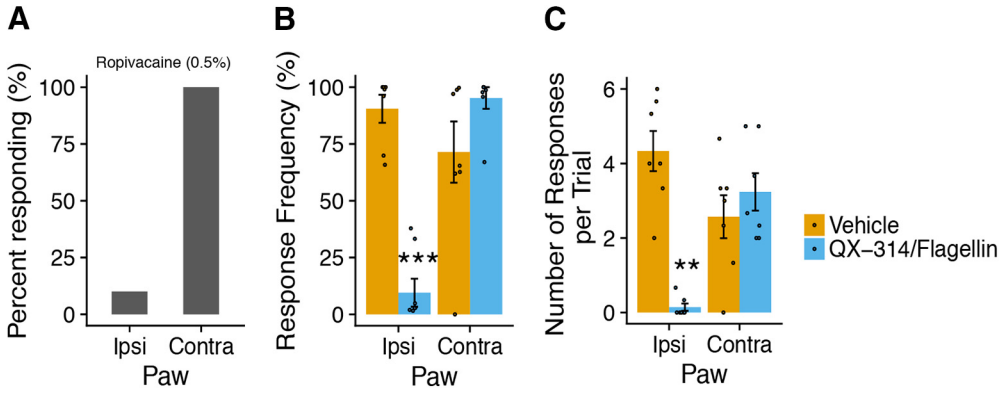

Figure 7. Local anesthetic and A-fiber selective blockade abolishes light-evoked paw withdrawal. ***A***, Intraplantar ropivacaine (0.5%, 20 μl) blocked light-evoked paw withdrawal in 8/9 mice ($n = 9$) in the ipsilateral (left) paw, but all mice (9/9) responsed to stimulation of the uninjected, contralateral paw. ***B***, Light-evoked response frequency was strongly attenuated in the ipsilateral paw of Vglut1-ChR2 mice that received A-fiber blockade with QX-314/flagellin (60 mM/1 μg, 20 μl, intraplantar, ipl) but not vehicle control (PBS, 20 μl, ipl) (treatment: $F_{(1,12)} = 13.58$, $p = 0.0031$, paw: $F_{(1,54)} = 8.00$, $p = 0.0066$, treatment × paw: $F_{(1,54)} = 20.3$, $p < 0.0001$). ***C***, Number of light-evoked responses was also strongly attenuated by QX-314/flagellin (treatment: $F_{(1,12)} = 12.88$, $p = 0.0037$, paw: $F_{(1,54)} = 1.05$, $p = 0.31$, treatment × paw: $F_{(1,54)} = 9.97$, $p = 0.0026$). For ***B*** and ***C***, in both treatment groups, the contralateral uninjected paw was stimulated after ipsilateral stimulation to demonstrate the localized nature of A-fiber blockade and to confirm the responsiveness of each subject ($n = 7$/group, stimulation: 5 mW/mm^2, 10 Hz). Statistical analysis: two-factor linear mixed effects (LME) model, Tukey's *post hoc* test. ***B*** and ***C*** are shown as means ± SEM. *Post hoc* test: $^{**}p < 0.01$, $^{***}p < 0.001$.

may be that activation of only a single subtype of Aβ-LTMR, either an RA- or SA-Aβ-LTMR, is needed to produce nociceptive behavior, and simultaneous coactivation of these two classes may actually interfere with one another; one class may be pro-nociceptive but the other could be anti-nociceptive, canceling one another and leading no net nociception.

Behavioral assays to assess pain-like behaviors

We measured reflexive paw withdrawal behaviors as well as real-time place aversion, approaches that have been used in the majority of similar optogenetic studies of primary sensory neurons (Draxler et al., 2014; Iyer et al., 2014, 2016; Beaudry et al., 2017) . With regard to withdrawal behaviors, our expectation was that, in the setting of nerve injury, either the number or character of the paw withdrawal behaviors would be altered. Similarly, because natural innocuous tactile stimuli can produce real-time aversion in the context of a sensitizing insult (Pratt et al., 2013), we also supposed that activating Vglut1-ChR2-positive neurons would produce aversion. We did not observe these expected outcomes. One explanation is that the behavioral assays that we used in this study may not have captured the true perceptual state of the animal, resulting in false-negative findings. That is, activation of

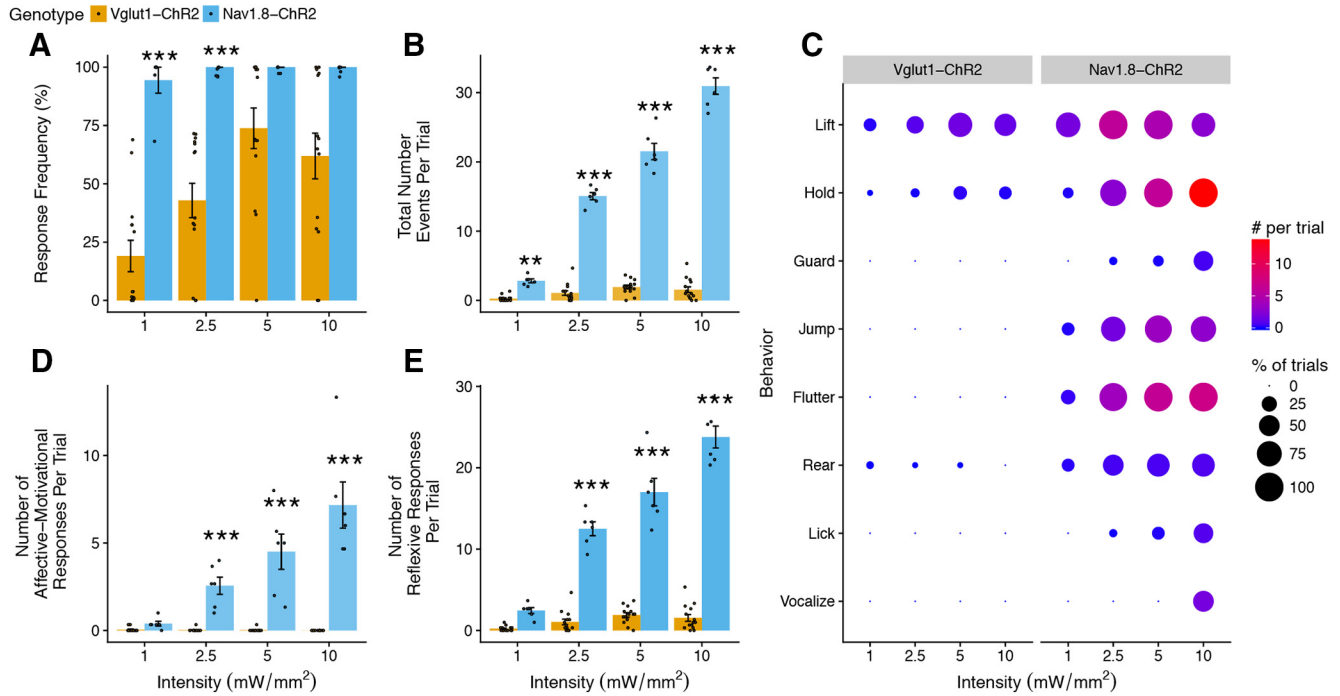

Figure 8. Comparison of light-evoked withdrawal behaviors in Vglut1-ChR2 and Nav1.8-ChR2 mice. ***A***, Response frequency of Vglut1-ChR2 is lower than that of Nav1.8-ChR2 at all intensities (genotype: $F_{(1,59)} = 51.99, p < 0.001$. intensity: $F_{(3,59)} = 11.07, p < 0.001$, genotype × intensity $F_{(3,59)} = 3.57, p = 0.02$). ***B***, Total number of responses is substantially lower in Vglut1-ChR2 compared with Nav1.8-ChR2 (genotype: $F_{(1,59)} = 2034.68, p < 0.001$, intensity: $F_{(3,59)} = 169.50, p < 0.001$, genotype × intensity: $F_{(3,59)} = 282.0273, p < 0.001$). ***C***, Behavioral signatures of Vglut1-ChR2 and Nav1.8-ChR2 differ markedly. Dot plot representation of individual scored behaviors at each intensity and frequency combination. The size of each dot represents the percentage of trials in which the behavior was observed, and the color represents the total number of a given behavior per trial, with red indicating higher numbers and blue indicating lower numbers. ***D***, Affective–motivational behaviors increase with intensity in Nav1.8-ChR2 but are absent in Vglut1-ChR2 (genotype: $F_{(1,59)} = 176.01, p < 0.001$, intensity: $F_{(3,59)} = 13.03, p < 0.001$, genotype × intensity: $F_{(3,59)} = 31.75, p < 0.001$). ***E***, Number of reflexive responses is higher at all intensities in Nav1.8-ChR2 (genotype: $F_{(1,59)} = 964.03, p < 0.001$, intensity: $F_{(3,59)} = 86.67, p < 0.001$, genotype × intensity: $F_{(3,59)} = 127.67, p < 0.001$). Statistical analysis: two-factor linear mixed effects (LME) model, Tukey's *post hoc* tests. Vglut1-Chr2, $n = 14$, and Nav1.8-ChR2, $n = 6$, for all panels. *Post hoc* tests: Vglut1-ChR2 versus Nav1.8-ChR2 at each intensity, $^{**}p < 0.01$, $^{***}p < 0.001$. ***A***, ***B***, ***D***, and ***E*** are shown as means ± SEM. The data presented here for Vglut1-ChR2 (2 Hz) are replotted from Figure 6.

Vglut1-ChR2-positive neurons may truly have been causing a painful perception during stimulation, but the features that we measured were not able to report on that perceptual state. Indeed, a recent report by Abdus-Saboor et al. used high-speed (1000 frames/s) video to analyze paw withdrawal responses to natural and optogenetic stimuli and found that the features that most strongly distinguished withdrawal to noxious stimuli from innocuous stimuli were paw height, paw velocity, and a composite "pain score," features that we were unable to measure in this study (Abdus-Saboor et al., 2018). Similarly, it may be the case that the relevant behavioral features or "syllables" that reflect the true underlying pain state are unrelated to anything we measured and instead should be discerned using unsupervised analysis, similar to the approach used by Wiltschko et al. (2015). Future studies applying these advanced behavioral methods to Vglut1-ChR2 mice may lead to different conclusions than the ones reached in this study.

Comparison with other optogenetic studies of LTMRs in pain

While preparing this manuscript, two studies were published that also examined the contribution of Aβ-LTMRs in pathological pain using optogenetics. Dhandapani et al. (2018) used a mouse expressing tamoxifen-inducible Cre recombinase in frame with TrkB (TrkB-CreERT2) to access a mixed population of PSNs composed of RA-Aβ-LTMRs and Aδ-LTMRs (D-hairs). They showed that, in the SNI model, TrkB-ChR2 mice showed increased response frequency at POD7 compared with baseline, along with the appearance of nocifensive responses to light (e.g., licking, prolonged lifting). Using toxin-mediated ablation, they also showed the necessity of *TrkB*-positive neurons for allodynia-like behaviors in the SNI model. We saw neither increased numbers of responses nor the appearance of nocifensive (i.e., affective–motivational) behaviors at POD7 in the SNI model using similar stimulation conditions. One likely explanation for the different behavioral findings in our study is that Vglut1-ChR2 does not access the neuronal population that caused the pain-like behaviors in the Dhandapani study. Although both TrkB-ChR2 and Vglut1-ChR2 label Ret-positive RA-Aβ-LTMRs, the Vglut1-ChR2 population does not overlap with the large majority of highly expressing *TrkB*-positive neurons ($TrkB^{High}$), which are most likely Aδ-LTMRs (Usoskin et al., 2015). Light stimulation of the sural territory inevitably shines on some hairy skin because the boundary between hairy and glabrous skin lies in this area. Thus, photostimulation of TrkB-positive Aδ-LTMRs may have occurred, giving rise to pain-like responses. It is therefore reasonable to suggest that Aδ-LTMRs mediated the positive pain-like behaviors in the Dhandapani et al. (2018) study in the SNI model. If true, then our study complements the findings from the Dhandapani study and suggests further refinement as to which population of LTMR is sufficient to elicit pain-like behaviors in nerve-injury-induced neuropathy.

Similarly, a study from Tashima et al. (2018) used an optogenetic approach to test the contribution of Aβ-LTMRs to pain-like behaviors in nerve-injury-induced neuropathy. They used a transgenic rat that expresses ChR2 broadly in non-nociceptive sensory neurons, some of which are Aβ-LTMRs, under the con-

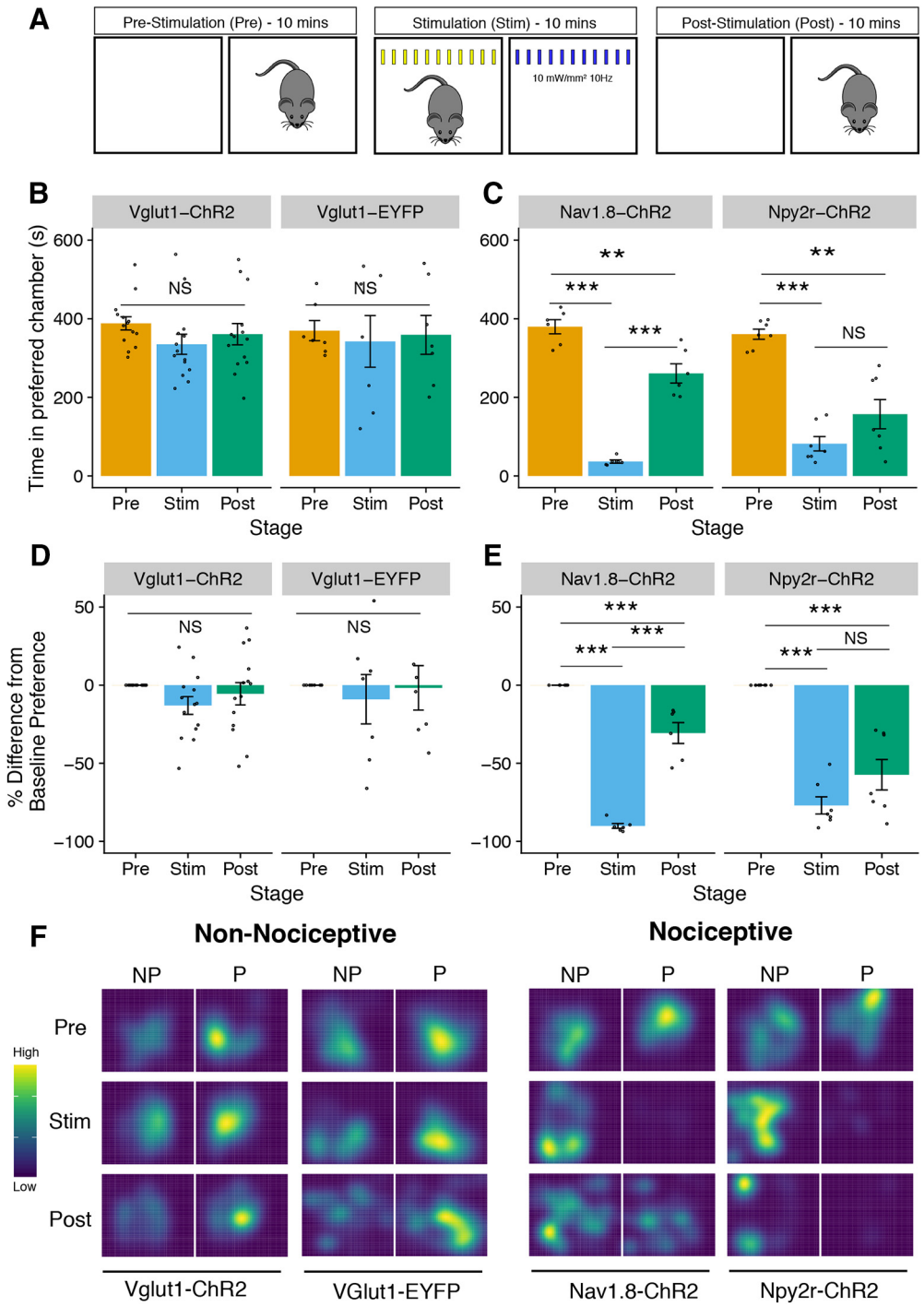

Figure 9. RT-PEA in non-nociceptive and nociceptive ChR2-expressing mouse line. ***A***, Schematic of RT-PEA assay. The assay is divided into three 10 min stages: prestimulation (Pre), stimulation (Stim), and poststimulation (Post). During the Pre period, mice are allowed to freely explore both sides of the chamber apparatus. During the Stim period, mice are stimulated with blue light in their preferred chamber and with yellow light in their nonpreferred chamber. During the Post period, mice freely moved between chambers without stimulation. ***B***, ***C***, Blue light stimulation causes strong aversion in nociceptive (Nav1.8-ChR2 and Npy2r-ChR2) but not non-nociceptive mice (Vglut1-ChR2 and Vglut1-EYFP). (Vglut1-ChR2, stage: $F_{(2,26)} = 2.44, p = 0.11, n = 14$. Vglut1-EYFP, stage: $F_{(2,12)} = 0.17, p = 0.85, n = 7$. Nav1.8-ChR2, stage: $F_{(2,10)} = 96.39, p < 0.0001, n = 6$, Npy2r-ChR2, stage: $F_{(2,12)} = 33.27, p < 0.0001, n = 7$). ***D***, ***E***, RT-PEA assay results represented as change from baseline (Pre) preference (%).(Vglut1-ChR2, stage: $F_{(2,26)} = 2.40, p = 0.11$. Vglut1-EYFP, stage: $F_{(2,12)} = 0.25, p = 0.78$. Nav1.8-ChR2, stage: $F_{(2,10)} = 144.8, p < 0.0001$, Npy2r-ChR2, stage: $F_{(2,12)} = 38.39, p < 0.0001$) . ***F***, Representative spatial heat maps for each mouse line. Yellow indicates more time spent in the area and blue indicates less time spent in the area. NP, Nonpreferred chamber; P, preferred chamber. Statistical analysis: one-factor linear mixed effects (LME) model for each line, with Tukey's *post hoc* test. *Post hoc* tests: $^{**}p < 0.01$, $^{***}p < 0.001$, NS, not significant ($p > 0.05$). ***B***–***E*** are shown as means ± SEM.

trol of the *Thy1* promoter (W-TChR2V4) (Ji et al., 2012) . They showed that, in rats that received unilateral peripheral nerve injury (spinal nerve transection model), photostimulation elicited pain-like behaviors on the ipsilateral paw but not on the contralateral paw. They also showed that injured rats exhibited light-evoked place aversion but naive rats did not. How to explain the discrepancy? First, light-evoked withdrawal in the uninjured paw "produced no reaction or only mild movement without any lift-

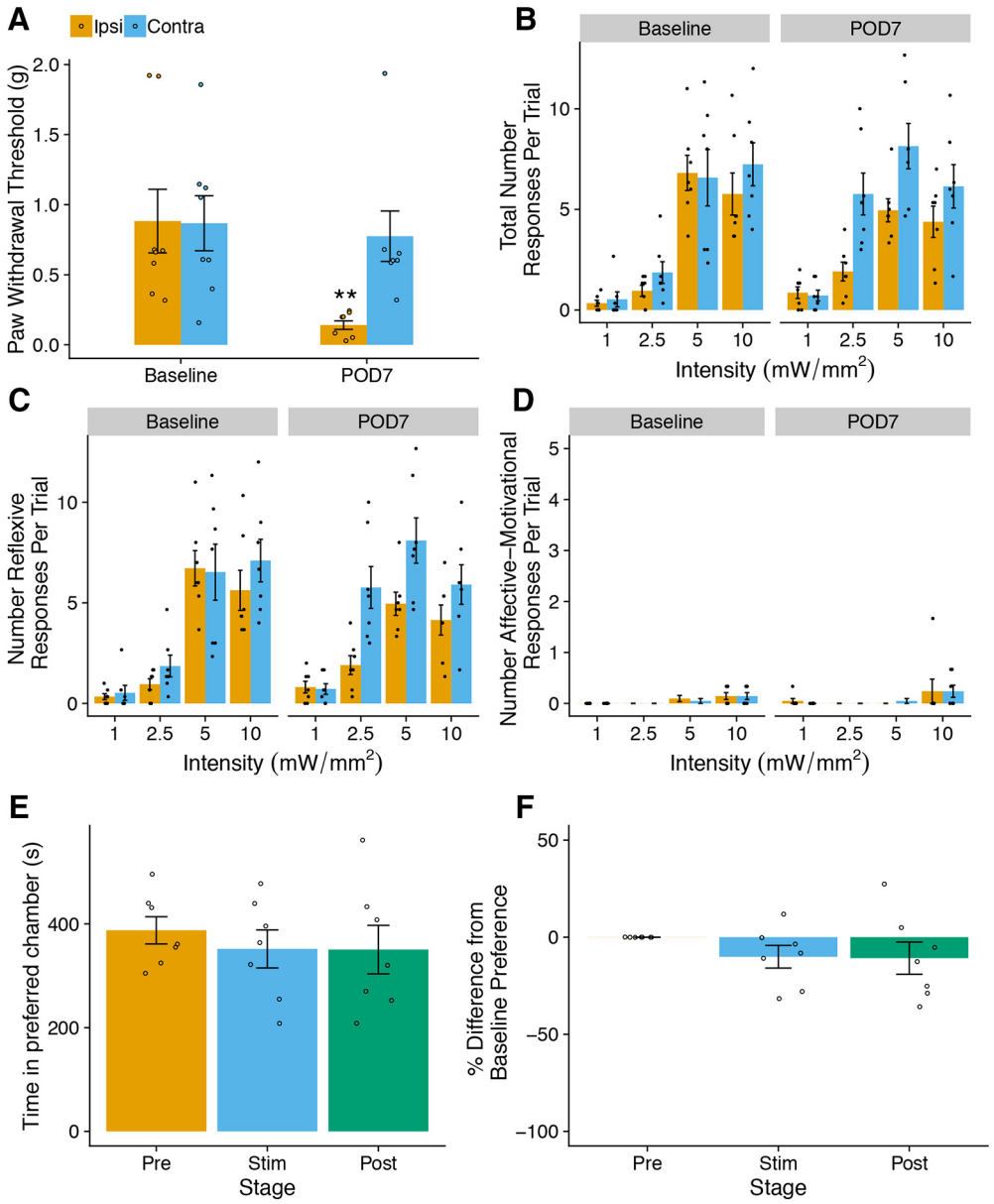

Figure 10. Optogenetic stimulation of SNI mice does not elicit pain-like behaviors or aversion. ***A***, SNI causes decreased PWTs in the ipsilateral paw on POD7 but not in the contralateral paw (n = 7 mice/group); two-factor linear mixed effects (LME), Tukey's *post hoc* test: paw: $F_{(1,18)} = 8.27$, $p = 0.01$, time point: $F_{(1,18)} = 11.92$, $p = 0.003$, paw × time point: $F_{(1,18)} = 13.99$, $p = 0.002$, *post hoc*: $^{**}p < 0.01$). ***B***, Total number of light-evoked responses is not significantly different between the ipsilateral and contralateral paws on POD7 (three-factor LME, paw: $F_{(1,90)} = 18.08$, $p = 0.0001$, time point: $F_{(1,90)} = 7.16$, $p = 0.009$, intensity: $F_{(3,90)} = 32.45$, $p < 0.0001$, paw × time point: $F_{(1,90)} = 0.28$, $p = 0.60$, paw × intensity: $F_{(3,90)} = 2.10$, $p = 0.11$, time point × intensity: $F_{(3,90)} = 1.59$, $p = 0.20$, paw × time point × intensity: $F_{(3,90)} = 1.43$, $p = 0.24$). ***C***, Number of reflexive responses is not different between ipsilateral and contralateral paws on POD7 (three-factor LME: paw: $F_{(1,90)} = 18.24$, $p < 0.0001$, time point: $F_{(1,90)} = 7.32$, $p = 0.008$, intensity: $F_{(3,90)} = 32.14$, $p < 0.0001$, paw × time point: $F_{(1,90)} = 0.31$, $p = 0.58$, paw × intensity: $F_{(3,90)} = 2.12$, $p = 0.10$, time point × intensity: $F_{(3,90)} = 1.61$, $p = 0.19$, paw × time point × intensity: $F_{(3,90)} = 1.50$, $p = 0.22$). ***D***, Number of affective–motivational responses is not different between ipsilateral and contralateral paws on POD7 (three-factor LME, paw: $F_{(1,90)} = 0.09$, $p = 0.77$, time point: $F_{(1,90)} = 0.0$, $p = 1.00$, intensity: $F_{(3,90)} = 5.71$, $p = 0.001$, paw × time point: $F_{(1,90)} = 0.08$, $p = 0.77$, paw × intensity: $F_{(3,90)} = 0.60$, $p = 0.61$, time point × intensity: $F_{(3,90)} = 0.29$, $p = 0.83$, paw × time point × intensity: $F_{(3,90)} = 0.26$, $p = 0.85$). ***E***, ***F***, Ipsilateral stimulation on POD7 did not produce more aversion compared with contralateral stimulation in a modified RT-PEA assay. One-factor LME, stage: $F_{(1,12)} = 0.98$, $p = 0.40$ (***E***) and $F_{(2,12)} = 1.06$, $p = 0.38$ (***F***). All plots are shown as means ± SEM.

ing or flinching behaviors" (Tashima et al., 2018), which presumably would also be true in naive animals. Accordingly, because the basal light-evoked behavior is a non-response, the changes that occurred on the injured paw were readily apparent and distinct. In contrast, in our study, even at the lowest intensity (1 mW/mm^2), the animals showed responses and at the higher intensities (5–10 mW/mm^2), they almost always responded, making it more challenging to see differences due to perturbations. Another key difference is the stimulation paradigm used by Tashima et al. (2018). They used relatively long pulse widths (500 ms) at very low frequency (0.1 Hz), whereas we used 5–10 ms pulse widths and 1–10 Hz pulsed stimulation, consistent with most other studies looking at peripheral optogenetic stimulation. We selected this stimulation protocol because it has been shown that continuous light causes ChR2 to desensitize (Nagel et al., 2003) and that long pulse-widths (>50 ms) can silence many kinds of neurons by inducing depolarization block (Herman et al., 2014). Indeed, we confirmed this using whole-cell patch-clamp in DRGs from

Vglut1-ChR2 mice *in vitro* using constant light, where only a single action potential was elicited at the onset of illumination followed by a constant, subthreshold depolarization. The nature of the electrophysiological effects *in vivo* caused by 500 ms pulses in the study by Tashima et al. (2018) are uncertain, but likely differed from ours. This difference may account for the divergent findings. Also, as mentioned for the Dhandapani et al. (2018) study, the populations of neurons accessed in the W-TChR2V4 rat may differ substantially from our Vglut1-ChR2 mouse. Furthermore, species differences (i.e., rat vs mouse) or differences in nerve injury model (SNI vs SNT) could account for our different findings. Regardless, this important study by Tashima et al. (2018) definitively demonstrated that a non-nociceptive population of LTMR can produce pain-like behaviors in specific contexts. Understanding and defining those contexts will be an important area of future investigation.

Despite these limitations, our study makes several interesting observations. The Vglut1-ChR2 mouse, as well as the Vglut1-Cre driver used to generate it, will be broadly useful for the study of pain and touch. Although there are numerous mouse lines to access various kinds of nociceptors (Cavanaugh et al., 2011), relatively few lines target Aβ-LTMRs. The Vglut1-Cre line expands the growing arsenal of Cre lines to target primary sensory neurons and complements the existing lines that access more restricted subpopulations of Aβ-LTMRs such as RetCreERT2 (Luo et al., 2009), TrkB-CreERT2 (Dhandapani et al., 2018), and TrkC-CreERT2 (Rutlin et al., 2014). The Vglut1-ChR2 mouse in particular could be used to study the contribution of LTMRs in other pain and itch conditions not tested here (e.g., inflammatory, chemotherapy). Furthermore, the Vglut1-Cre line can be used to express other opsins or fluorophores or for the conditional manipulation of natively expressed genes. The intensive behavioral characterization that we performed sheds light on the different behavioral signatures of non-nociceptive and nociceptive neuronal activation and highlights the importance of measuring features beyond just paw lifting, which is a seemingly universal response across optogenetic mouse lines (Draxler et al., 2014; Iyer et al., 2014, 2016; Beaudry et al., 2017). The RT-PEA assay that we adapted expands the arsenal of ways that one can use transdermal optogenetics to study pain and will be useful in the study of other optogenetic lines. Finally, at least in the case of the SNI model, our findings refine our understanding of the contribution of Aβ-LTMRs to neuropathic pain.

References

Abraira VE, Ginty DD (2013) The Sensory Neurons of Touch. Neuron 79:618–639.

Abdus-Saboor I, Fried NT, Lay M, Dong P, Burdge J, Lu M, Ma M, Dong X, Long D, Luo W (2018) High-speed imaging of paw withdrawal reflex to objectively Assess pain state in mice. bioRxiv. Advance online publication. Retrieved February 12, 2018. doi:10.1101/263400.

Agarwal N, Offermanns S, Kuner R (2004) Conditional gene deletion in primary nociceptive neurons of trigeminal ganglia and dorsal root ganglia. genesis 38:122–129.

Alvarez FJ, Villalba RM, Zerda R, Schneider SP (2004) Vesicular glutamate transporters in the spinal cord, with special reference to sensory primary afferent synapses. J Comp Neurol 472:257–280.

Arcourt A, Gorham L, Dhandapani R, Prato V, Taberner FJ, Wende H, Gangadharan V, Birchmeier C, Heppenstall PA, Lechner SG (2017) Touch receptor-derived sensory information alleviates acute pain signaling and fine-tunes nociceptive reflex coordination. Neuron 93:179–193.

Bai L, Lehnert BP, Liu J, Neubarth NL, Dickendesher TL, Nwe PH, Cassidy C, Woodbury CJ, Ginty DD (2015) Genetic identification of an expansive mechanoreceptor sensitive to skin stroking. Cell 163:1783–1795.

Bankhead P, Loughrey MB, Fernández JA, Dombrowski Y, McArt DG, Dunne PD, McQuaid S, Gray RT, Murray LJ, Coleman HG, James JA, Salto-Tellez M, Hamilton PW (2017) QuPath: open source software for digital pathology image analysis. Sci Rep 7:16878.

Basbaum AI, Bautista DM, Scherrer G, Julius D (2009) Cellular and molecular mechanisms of pain. Cell 139:267–284.

Beaudry H, Daou I, Ase AR, Ribeiro-da-Silva A, Séguéla P (2017) Distinct behavioral responses evoked by selective optogenetic stimulation of the major TRPV1+ and MrgD+ subsets of C-fibers. PAIN 158:2329–2339.

Berta T, Perrin FE, Pertin M, Tonello R, Liu Y-C, Chamessian A, Kato AC, Ji RR, Decosterd I (2017) Gene expression profiling of cutaneous injured and non-Injured nociceptors in SNI animal model of neuropathic pain. Sci Rep 7:9367.

Bonin RP, Bories C, De Koninck Y (2014) A simplified up-down method (SUDO) for measuring mechanical nociception in rodents using von Frey filaments. Mol Pain 10:26.

Bourane S, Garces A, Ventéo S, Pattyn A, Hubert T, Fichard A, Puech S, Boukhaddaoui H, Baudet C, Takahashi S, Valmier J, Carroll P (2009) Low-threshold mechanoreceptor subtypes selectively express MafA and are specified by ret signaling. Neuron 64:857–870.

Bourquin AF, Süveges M, Pertin M, Gilliard N, Sardy S, Davison AC, Spahn DR, Decosterd I (2006) Assessment and analysis of mechanical allodynia-like behavior induced by spared nerve injury (SNI) in the mouse. PAIN 122:14.e1–e14.

Brumovsky P, Watanabe M, Hökfelt T (2007) Expression of the vesicular glutamate transporters-1 and -2 in adult mouse dorsal root ganglia and spinal cord and their regulation by nerve injury. Neuroscience 147:469–490.

Cavanaugh DJ, Chesler AT, Jackson AC, Sigal YM, Yamanaka H, Grant R, O'Donnell D, Nicoll RA, Shah NM, Julius D, Basbaum AI (2011) Trpv1 reporter mice reveal highly restricted brain distribution and functional expression in arteriolar smooth muscle cells. J Neurosci 31:5067–5077.

Chang RB, Strochlic DE, Williams EK, Umans BD, Liberles SD (2015) Vagal sensory neuron subtypes that differentially control breathing. Cell 161:622–633.

Corder G, Tawfik VL, Wang D, Sypek EI, Low SA, Dickinson JR, Sotoudeh C, Clark JD, Barres BA, Bohlen CJ, Scherrer G (2017) Loss of μ opioid receptor signaling in nociceptors, but not microglia, abrogates morphine tolerance without disrupting analgesia. Nat Med 23:164–173.

da Silva Serra I, Husson Z, Bartlett JD, Smith ESJ (2016) Characterization of cutaneous and articular sensory neurons. Mol Pain 12:174480691663638.

Daou I, Tuttle AH, Longo G, Wieskopf JS, Bonin RP, Ase AR, Wood JN, De Koninck Y, Ribeiro-da-Silva A, Mogil JS, Séguéla P (2013) Remote optogenetic activation and sensitization of pain pathways in freely moving mice. J Neurosci 33:18631–18640.

Dhandapani R, Arokiaraj CM, Taberner FJ, Pacifico P, Raja S, Nocchi L, Portulano C, Franciosa F, Maffei M, Hussain AF, de Castro Reis F, Reymond L, Perlas E, Garcovich S, Barth S, Johnsson K, Lechner SG, Heppenstall PA (2018) Control of mechanical pain hypersensitivity in mice through ligand-targeted photoablation of TrkB-positive sensory neurons. Nat Commun 9:1640.

Draxler P, Honsek SD, Forsthuber L, Hadschieff V, Sandkühler J (2014) VGluT3 primary afferents play distinct roles in mechanical and cold hypersensitivity depending on pain etiology. J Neurosci 34:12015–12028.

Smith ES, Lewin GR (2009) Nociceptors: a phylogenetic view. J Comp Physiol A Neuroethol Sens Neural Behav Physiol 195:1089–1106.

Friard O, Gamba M (2016) BORIS: a free, versatile open-source event-logging software for video/audio coding and live observations. Methods in Ecology and Evolution 7:1325–1330.

Harris JA, Hirokawa KE, Sorensen SA, Gu H, Mills M, Ng LL, Bohn P, Mortrud M, Ouellette B, Kidney J, Smith KA, Dang C, Sunkin S, Bernard A, Oh SW, Madisen L, Zeng H (2014) Anatomical characterization of Cre driver mice for neural circuit mapping and manipulation. Front Neural Circuits 8:76.

Herman AM, Huang L, Murphey DK, Garcia I, Arenkiel BR (2014) Cell type-specific and time-dependent light exposure contribute to silencing in neurons expressing Channelrhodopsin-2. eLife 3:e01481.

Iyer SM, Montgomery KL, Towne C, Lee SY, Ramakrishnan C, Deisseroth K, Delp SL (2014) Virally mediated optogenetic excitation and inhibition of pain in freely moving nontransgenic mice. Nat Biotechnol 32:274–278.

Iyer SM, Vesuna S, Ramakrishnan C, Huynh K, Young S, Berndt A, Lee SY, Gorini CJ, Deisseroth K, Delp SL (2016) Optogenetic and chemogenetic strategies for sustained inhibition of pain. Sci Rep 6:30570.

Ji ZG, Ito S, Honjoh T, Ohta H, Ishizuka T, Fukazawa Y, Yawo H (2012)

Light-evoked Somatosensory Perception of Transgenic Rats That Express Channelrhodopsin-2 in Dorsal Root Ganglion Cells Baccei ML, ed. PLoS ONE 7:e32699.

Latremoliere A, Woolf CJ (2009) Central sensitization: a generator of pain hypersensitivity by central neural plasticity. The Journal of Pain 10:895–926.

Lolignier S, Eijkelkamp N, Wood JN (2015) Mechanical allodynia. Pflugers Arch 467:133–139.

Luo W, Enomoto H, Rice FL, Milbrandt J, Ginty DD (2009) Molecular identification of rapidly adapting mechanoreceptors and their developmental dependence on ret signaling. Neuron 64:841–856.

Madisen L, Mao T, Koch H, Zhuo JM, Berenyi A, Fujisawa S, Hsu YW, Garcia AJ 3rd, Gu X, Zanella S, Kidney J, Gu H, Mao Y, Hooks BM, Boyden ES, Buzsáki G, Ramirez JM, Jones AR, Svoboda K, Han X et al. (2012) A toolbox of cre-dependent optogenetic transgenic mice for light-induced activation and silencing. Nat Neurosci 15:793–802.

Madisen L, Zwingman TA, Sunkin SM, Oh SW, Zariwala HA, Gu H, Ng LL, Palmiter RD, Hawrylycz MJ, Jones AR, Lein ES, Zeng H (2010) A robust and high-throughput cre reporting and characterization system for the whole mouse brain. Nat Neurosci 13:133–140.

Nagel G, Szellas T, Huhn W, Kateriya S, Adeishvili N, Berthold P, Ollig D, Hegemann P, Bamberg E (2003) Channelrhodopsin-2, a directly light-gated cation-selective membrane channel. Proc Natl Acad Sci U S A 100:13940–13945.

Pratt D, Fuchs PN, Sluka KA (2013) Assessment of avoidance behaviors in mouse models of muscle pain. Neuroscience 248:54–60.

Rodriguez E, Sakurai K, Xu J, Chen Y, Toda K, Zhao S, Han BX, Ryu D, Yin H, Liedtke W, Wang F (2017) A craniofacial-specific monosynaptic circuit enables heightened affective pain. Nat Neurosci 20:1734–1743.

Rogoz K, Lagerström MC, Dufour S, Kullander K (2012) VGLUT2-dependent glutamatergic transmission in primary afferents is required for intact nociception in both acute and persistent pain modalities. PAIN 153:1525–1536.

Rutlin M, Ho CY, Abraira VE, Cassidy C, Bai L, Woodbury CJ, Ginty DD (2014) The cellular and molecular basis of direction selectivity of Aδ-LTMRs. Cell 159:1640–1651.

Srinivas S, Watanabe T, Lin CS, William CM, Tanabe Y, Jessell TM, Costantini F (2001) Cre reporter strains produced by targeted insertion of EYFP and ECFP into the ROSA26 locus. BMC Dev Biol 1:4.

Tashima R, Koga K, Sekine M, Kanehisa K, Kohro Y, Tominaga K, Matsushita K, Tozaki-Saitoh H, Fukazawa Y, Inoue K, Yawo H, Furue H, Tsuda M (2018) Optogenetic activation of non-nociceptive Aβ fibers induces neuropathic pain-like sensory and emotional behaviors after nerve injury in rats. eNeuro 5:ENEURO.0450–17.2018.

Todd AJ, Hughes DI, Polgár E, Nagy GG, Mackie M, Ottersen OP, Maxwell DJ (2003) The expression of vesicular glutamate transporters VGLUT1 and VGLUT2 in neurochemically defined axonal populations in the rat spinal cord with emphasis on the dorsal horn. Eur J Neurosci 17:13–27.

Torebjörk HE, Lundberg LE, LaMotte RH (1992) Central changes in processing of mechanoreceptive input in capsaicin-induced secondary hyperalgesia in humans. The Journal of Physiology 448:765–780.

Usoskin D, Furlan A, Islam S, Abdo H, Lönnerberg P, Lou D, Hjerling-Leffler J, Haeggström J, Kharchenko O, Kharchenko PV, Linnarsson S, Ernfors P (2015) Unbiased classification of sensory neuron types by large-scale single-cell RNA sequencing. Nat Neurosci 18:145–153.

Williams WO, Riskin DK, Mott AKM (2008) Ultrasonic sound as an indicator of acute pain in laboratory mice. J Am Assoc Lab Anim Sci 2008;47:8–10.

Wiltschko AB, Johnson MJ, Iurilli G, Peterson RE, Katon JM, Pashkovski SL, Abraira VE, Adams RP, Datta SR (2015) Mapping sub-second structure in mouse behavior. Neuron 88:1121–1135.

Xu ZZ, Kim YH, Bang S, Zhang Y, Berta T, Wang F, Oh SB, Ji RR (2015) Inhibition of mechanical allodynia in neuropathic pain by TLR5-mediated A-fiber blockade. Nat Med 21:1326–1331.

Zimmerman A, Bai L, Ginty DD (2014) The gentle touch receptors of mammalian skin. Science 346:950–954.